Title	Modeling Network Interference in the Angular Domain: Interference Azimuth Spectrum
Author(s)	Chen, Y.; Mucchi, L.; Wang, R.; Huang, K
Citation	IEEE Transactions on Communications, 2014, v. 62, p. 2107-2120
Issued Date	2014
URL	http://hdl.handle.net/10722/200612
Rights	Creative Commons: Attribution 3.0 Hong Kong License

Modeling Network Interference in the Angular Domain: Interference Azimuth Spectrum

Yifan Chen, *Member, IEEE*, Lorenzo Mucchi, *Senior Member, IEEE*,
Rui Wang, and Kaibin Huang, *Senior Member, IEEE*

***Abstract*—The performance of wireless networks is fundamentally limited by interference [or, equivalently, the signal-to-interference ratio (SIR)]. In an attempt to characterize the interference as a direction-selective quantity and motivated by the useful analogy between classical propagation channels and wireless networks, we propose a novel network description framework, namely the interference azimuth spectrum (IAS). The IAS represents the distribution of interference in the angular domain and is parallel to the conventional power azimuth spectrum (PAS) used in propagation channels. We also extend this concept to the directional characterization of average achievable rate, assuming that interference is treated as noise. Provided with this analytical framework, we present the notion of local area outage, defined as the probability that a receiver is in the state of outage within a local area where both interference and desired signal are assumed to be wide-sense stationary (WSS). We further propose the geometry-based stochastic models (GBSMs) as a part of the IAS framework, where the interfering terminals are randomly distributed according to a specific probability density function (pdf) of their positions. The GBSMs are applicable to a wide variety of wireless network environments without and with interferer clustering. The proposed methodology would provide useful insight on the design and performance assessment of future networks, featured by opportunistic, randomized, and dense placement of nodes.**

***Index Terms*—Achievable rate, coverage, directional characterization, geometry-based stochastic models, interference modeling.**

I. Introduction

In large-scale wireless networks comprising many spatially scattered nodes, dense spatial reuse of the available radio spectrum is required to achieve efficient spectral usage. Hence, it is impossible to separate concurrent transmissions completely in frequency. This causes severe network interference where signals from many undesired transmitters are aggregated at a receiver. As many emerging classes of wireless systems such as *ad hoc*, sensor, cognitive, and heterogeneous cellular networks require decentralized channelization, power control, and resource allocation, interference becomes the main performance bottleneck in these systems. The modeling of network interference is thus critical to the analysis and design of communication systems such as the development of interference avoidance and power control techniques.

A. Related Work and Motivation

Network interference is basically affected by the spatial distribution of interferers [1]–[8]. Conventional deterministic models include square, triangular, and hexagonal lattices in the two-dimensional plane [9]–[13]. However, the grid models have the serious drawback in terms of their accuracy and tractability for the heterogeneous and *ad hoc* deployment commonly encountered in urban and suburban areas. An emerging approach is to describe the distribution of active interferers in large random wireless networks as a homogeneous spatial Poisson point process [1]. Such a simple model allows useful mathematical tools from stochastic geometry to be applied for tractable and relatively accurate analysis of wireless networks [14]. The models have been generalized to account for repulsion or minimum distance between transmitting nodes, such as a modified Matern hard-core point process [5]. A guard zone around the typical receiver in a Poisson model is also introduced to model the effect of contention- or scheduling-based medium access control (MAC) protocols [2]. Furthermore, Poisson clustered processes are employed to characterize clustering of interferers due to geographical factors or introduced intentionally by the MAC protocol [2], [7]. Very recently, temporal correlation in network interference has been accounted for along the same line of thought [15]. Nevertheless, these point processes do not provide insight on the direction-selective interference power at an arbitrary receiver. Hence, they do not fully exploit the benefits of employing advanced angle-resolved or spatial-diversity systems in wireless networks. This motivates characterizing interference statistics in the angular domain. We will approach this problem by utilizing a novel analogy between classical wireless propagation channels and interference networks.

Consider the wireless medium shown in Fig. 1(a), which comprises a set of propagation paths delivering signal power from a transmitter to a receiver via various scatterers (e.g., building, tree, person). We focus on the single-bounce scenario, where each path undergoes only one reflection at the corresponding scatterer. The principle underpinning our interference

Manuscript received August 10, 2013; revised December 25, 2013; accepted March 24, 2014. Date of publication April 2, 2014; date of current version June 18, 2014. This work was supported in part by the EU FP7 Marie Curie International Research Staff Exchange Scheme under Grant 294923 and by the 2013 Guangdong Natural Science Funds for Distinguished Young Scholar under Grant S2013050014223. The associate editor coordinating the review of this paper and approving it for publication was O. Oyman.

Y. Chen and R. Wang are with the Department of Electrical and Electronic Engineering, South University of Science and Technology of China, Shenzhen 518055, China (e-mail: chen.yf@sustc.edu.cn; wang.r@sustc.edu.cn).

L. Mucchi is with the Department of Electronics and Telecommunications, University of Florence, 50139 Florence, Italy (e-mail: lorenzo.mucchi@unifi.it).

K. Huang is with the Department of Electrical and Electronic Engineering, University of Hong Kong, Hong Kong, China (e-mail: huangkb@ieee.org).

Color versions of one or more of the figures in this paper are available online at http://ieeexplore.ieee.org.

Digital Object Identifier 10.1109/TCOMM.2014.2314651

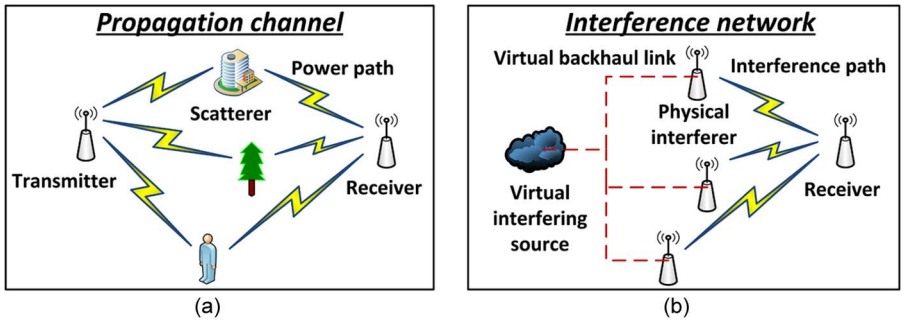

Fig. 1. Analogy between (a) propagation channel and (b) interference network.

modeling approach is that, *an interference network itself is the channel* as also revealed in Fig. 1(b). We can introduce a *virtual* interfering source connected to multiple *physical* interferers through *virtual* backhaul links. The source generates an interfering signal and the backhaul links introduce propagation delays which are dependent on the emerging times of the physical interferers. These interferers amplify and forward like relays the incoming signals from the source. They serve as the interference delivery medium, which is parallel to scatterers in propagation channels as signal power reflectors.

This analogy inspires us to look into more specific aspects of interference network characterization. In propagation channels, the directional impulse response (DIR) is widely regarded as the fundamental description method, which depends on delay, angle-of-arrival (AOA), and number of multipath components [16]. We can thus derive the DIR for interference networks following the analogy mentioned above. Subsequently, we can obtain important interference statistics related to the DIR and the average data rate experienced by a mobile receiver in a local area, where both interference and desired signal are assumed to be wide-sense stationary (WSS). Furthermore, the geometry-based stochastic model (GBSM) is commonly employed as a mathematical abstraction of propagation channels [16]. The GBSM assigns locations to scatterers according to the probability density function (pdf) of their positions. The GBSM has the advantages of reducing computational load, improving prediction accuracy, and facilitating closed-form theoretical analysis. Furthermore, it is particularly useful when movement is to be simulated [16]. This is because whenever the transmitter, receiver or scatterers move, the parameters of propagation paths are adjusted automatically. Similarly, we can apply the GBSM to characterize the spatial distribution of interfering radios, which leads to trackable expressions of interference distributions in the angular domain for various network scenarios. As such, the GBSM supports and enriches the description method mentioned above.

B. Main Contributions and Organization

In this paper, we propose the notion of interference azimuth spectrum (IAS), which is analogous to the conventional description method of power azimuth spectrum (PAS) in propagation channels. Subsequently, we present the fundamental second-order small-scale fading statistics, including level crossing rate (LCR), average fade distance (AFD), spatial autocovariance, and coherence distance, for interference fluctuations at a mobile receiver traveling through a local area. These quantities find their counterparts in directional propagation channels. Furthermore, built on this analogy, we obtain the new expressions of LCR, AFD, autocovariance, and coherence distance for the signal-to-interference ratio (SIR) fluctuations, assuming that the thermal noise is negligible [6]. This assumption can be easily relaxed at the cost of much more complicated derivations without offering new insight. Furthermore, we compute the ergodic rate $\mathbb{E}[\log(1+\mathrm{SIR})]$ experienced by a mobile receiver when the antenna boresight points towards various directions, assuming that interference is treated as noise, which results in the average rate azimuth spectrum (ARAS). The quantity becomes the actual bandwidth-normalized capacity in the Gaussian weak interference regime. Given ARAS, we introduce the concept of local area outage, which is defined as the probability that the average data rate achieved at a mobile moving through the local area with a random antenna boresight is below a pre-defined threshold value. This allows us to determine the forbidden zone of interference (FZI) in the global service area. The FZI provides information about the area where the rate is significantly compromised due to interference.

The paper is structured as follows. In Section II, we discuss the system model and construct the one-to-one correspondence between the essential elements constituting a propagation channel and an interference network. In Section III, we derive the IAS and the second-order statistics of interference and SIR. In Section IV, we present the notions of ARAS, local area outage, and FZI. In Section V, we analyze the GBSM applicable to generic interferer clustering scenarios and derive the IAS. In Section VI, we exemplify some properties of the proposed modeling paradigm through several numerical examples. Finally, we draw some concluding remarks in Section VII.

II. Signal Model

Consider a two-dimensional propagation channel, where there are K scatterers, $\mathcal{S}_1, \mathcal{S}_2, \ldots, \mathcal{S}_K$ between a transmitter $\mathcal{T}$ and a receiver $\mathcal{R}$ as illustrated in Fig. 2. It is assumed that the dimensions of these objects are small relative to the system spatial resolution (i.e., point scatterer assumption). Signal propagates from $\mathcal{T}$ to $\mathcal{R}$ via multiple paths that involve single-bounce scattering, i.e., $\mathcal{T} \to \mathcal{S}_k \to \mathcal{R}$ with $k = 1, 2, \ldots, K$.

Parallel to the above scenario, we may consider a generic large-scale wireless network with K interfering radios scattered over a wide region, $\mathbf{I}_1, \mathbf{I}_2, \ldots, \mathbf{I}_K$, and an interfered receiver $\mathbf{R}$. We further assume that the transmit power of $\mathbf{I}_k (k = 1, 2, \ldots,$

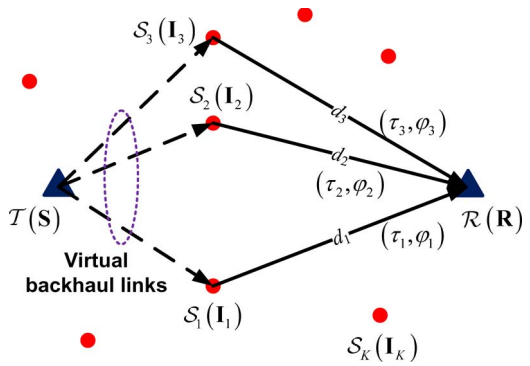

Fig. 2. Bijection between propagation channel and interference network: Scatterer $\mathcal{S} \longleftrightarrow$ Physical interferer $\mathbf{I}$, Transmitter $\mathcal{T} \longleftrightarrow$ Virtual interfering source $\mathbf{S}$, Receiver $\mathcal{R} \longleftrightarrow$ Receiver $\mathbf{R}$.

K) is P_k. For ease of understanding, we can replace this multiple-source, single-destination system with an equivalent single-source, single-destination interference network by introducing a virtual interfering source $\mathbf{S}$ as shown in Fig. 2. $\mathbf{S}$ transmits a unit-power *imaginary* signal, which is "scattered" from each physical interferer $\mathbf{I}_k$ with an average scattering coefficient of $\sqrt{P_k}$, and impinges on the receiver $\mathbf{R}$.

As shown in Fig. 2, the kth $(k = 1, 2, \ldots, K)$ path introduces a delay τ_k and an AOA φ_k for either the propagation channel or the interference network. In the former case, the term τ_k corresponds to the actual time-of-arrival, which is proportional to the propagation distance of each multipath component $\mathcal{T} \to \mathcal{S}_k \to \mathcal{R}$. However, in the latter case the delay $\tau_k = \tau_k' + d_k/c$, where τ_k' is the transmission time of $\mathbf{I}_k$, d_k is the distance between $\mathbf{I}_k$ and $\mathbf{R}$ (see Fig. 2), and c is the speed of electromagnetic waves. The term τ_k' can be interpreted as the delay of the virtual backhaul link $\mathbf{S} \to \mathbf{I}_k$. We assume a fully decentralized wireless network where interfering radios are independent and non-coordinated, and thus can start to transmit at any time. Note that scatterers in propagation channels are passive objects and their structure (e.g., a large building which consists of multiple interconnected scatterers) may result in correlation between arriving times and angles of multipath at the receiver. On the other hand, physical interferers in interference networks are active terminals, which are generally independent from each other during the transmission process.

III. Azimuthal Spectrum and Second-Order Statistics of Interference

A. Angular Spectrum of Interfering Signal

Following from Section II, the interfering signal observed at an arbitrary receiver $\mathbf{R}$ is distributed in the azimuth-delay domain. Hence, the DIR widely used in describing propagation channels can be applied to interference networks, which consists of the sum of contributions from all interfering radios

$$h_I(\tau,\varphi) = \sum_{k=1}^{K} h_{I,k}\delta(\tau-\tau_k)\delta(\varphi-\varphi_k) \tag{1}$$

where the subscript I indicates interference throughout the paper, $h_{I,k} = \sqrt{\alpha_k P_k} d_k^{-n_{\mathrm{PL}}/2}\beta_k e^{j\theta_k}$ is the scaling coefficient of the kth path, $\alpha_k P_k$ is the average power measured 1 m away from the kth interferer, n_{PL} is the power path loss exponent, and $\beta_k e^{j\theta_k}$ is the distortion due to fading experienced by the interferer emission. The impulse response depends on delay τ, AOA φ, and path number K. Random variables β_k and θ_k are assumed to be identically and independently distributed (i.i.d.) for each interferer $\mathbf{I}_k$.

Analogous to the analysis of propagation channels, we can present the condensed descriptions of the interference network performance metrics. The most fundamental quantity is the interference delay-azimuth spectrum (IDAS):

$$\Xi_I^{(\mathrm{IDAS})}(\tau,\varphi) = \sum_{k=1}^{K} |h_{I,k}|^2\delta(\tau-\tau_k)\delta(\varphi-\varphi_k). \tag{2}$$

The terminology *azimuth-delay spectrum* is adopted according to [17]. Following (2), the IAS is derived as

$$\begin{aligned}\Xi_I^{(\mathrm{IAS})}(\varphi) &= \int_{\tau} \mathbb{E}\left[\Xi_I^{(\mathrm{IDAS})}(\tau,\varphi)\right] \mathrm{d}\tau \\ &\propto \int_{\tau} \mathbb{E}\left[|h_I|^2|\tau,\varphi\right] f_{\tau,\varphi}(\tau,\varphi)\mathrm{d}\tau.\end{aligned} \tag{3}$$

$\mathbb{E}[|h_I|^2|\tau,\varphi] = \mathbb{E}[|h_{I,k}|^2|\tau_k=\tau,\varphi_k=\varphi]$ is the expected received power of the kth interference path conditioned on its delay and AOA. $f_{\tau,\varphi}(\tau,\varphi)$ is the joint pdf of delay and AOA. The proportionality applies to the ensemble average of many spatial realizations of the network, whose nodes are placed according to some probability distribution, such that the directional description can be expressed as a continuous spectrum. This representation captures the decentralized, randomized, and dense placement of nodes in many emerging classes of large wireless systems. The IAS is parallel to the definition of PAS in propagation channels and is usually normalized as $\int_{\varphi} \Xi_I^{(\mathrm{IAS})}(\varphi)\mathrm{d}\varphi = 1$.

To characterize the amount of interference dispersion in the azimuthal domain by measuring the width of IAS, we adapt the angular spread used in the classical definition [18]:

$$\sigma_I = \sqrt{\int_{\varphi} |\exp(j\varphi) - \mu_\varphi|^2 \, \Xi_I^{(\mathrm{IAS})}(\varphi)\mathrm{d}\varphi} \tag{4}$$

where

$$\mu_\varphi = \int_{\varphi} \exp(j\varphi)\Xi_I^{(\mathrm{IAS})}(\varphi)\mathrm{d}\varphi. \tag{5}$$

If an interference network is quasi-static, i.e., the durations of IDAS and interfering signal are much shorter than the time over which the network changes significantly, we can consider the behavior of the network at one time like that of a linear time-invariant system. Consequently, both the deterministic and stochastic system functions used for propagation channels in [16] can also be applied to such networks. We can thus define the WSS interfering condition (analogous to the WSS assumption in propagation channels) through simplification of the autocorrelation function of DIR. Within a local area, both interference and desired signal are assumed to be WSS and their

angular distributions remain unchanged. This basic property underlies all the following discussions.

B. Level Crossing

1) LCR of Interference: With an understanding of IAS, it is possible to derive many basic second-order statistical measures of a fluctuating interference channel. The most common approach is to model the channel by a Gaussian random process. This is appropriate when the interference is the accumulation of a large number of independent signals, where no term dominates the sum, and thus the central limit theorem applies. Non-Gaussian interference model for fading channels has also been considered, which has some advantage in predicting the bit error probability performance [19]. Recent investigations have seen more complex models for the interference statistics from a field of Poisson and Poisson-Poisson clustered distributed interferers (e.g., the symmetric alpha stable and Gaussian mixture models [2]). The current derivations focus on the Nakagami-m distribution for its ease of manipulation and wide range of applicability, which generalizes the Rayleigh and one-sided Gaussian distributions and approximates the lognormal, Hoyt, and Rician distributions, commonly used in wireless channel modeling [20], [21]. Furthermore, the sum of multiple i.i.d. Rayleigh-fading interference signals [22], [23] have a Nakagami-m distributed signal amplitude. This is particularly relevant to model interference from multiple sources in a wireless network [24]. Additionally, the aggregate interference power from multiple unintended transmitters was often approximated by a Gamma distribution (see e.g., [25]–[27]). If we define the amplitude to be proportional to the square root of the power, then the amplitude of this aggregate interference has a Nakagami-m distribution.

Subsequently, the fading interference envelope r_I has the following pdf:

$$f_{r_I}(r_I) = \frac{2m_I^{m_I} r_I^{2m_I-1}}{\Gamma(m_I) P_I^{m_I}} \exp\left(-\frac{m_I r_I^2}{P_I}\right) \tag{6}$$

where $P_I = \mathbb{E}[r_I^2]$ is the average interference power in a local area, $m_I = \mathbb{E}^2[r_I^2]/\mathrm{var}(r_I^2)$ is the shape factor, and $\Gamma(\cdot)$ is the Gamma function.

Consider a receiver traveling along a fixed azimuthal direction φ_0. The corresponding stochastic process of fading interference is a function of space. We can thus define the LCR $N_I(R_I)$ as the average number of crossings per unit distance that the process drops beneath a specified threshold level. The general expression of LCR is given by

$$N_I(R_I) = \int_0^\infty \dot{r}_I f_{r_I,\dot{r}_I}(r_I = R_I, \dot{r}_I) \mathrm{d}\dot{r}_I \tag{7}$$

where R_I is the threshold level for interference crossing and $f_{r_I,\dot{r}_I}(R_I, \dot{r}_I)$ is the joint pdf of envelope and its time derivative. For a Nakagami-m fading signal, the LCR is [28]

$$N_I(\rho_I) = \frac{\sigma_{V_I}}{\sqrt{\pi P_I}} \frac{m_I^{m_I-1/2}}{\Gamma(m_I)} \rho_I^{2m_I-1} \exp\left(-m_I \rho_I^2\right). \tag{8}$$

The variable ρ_I is the normalized threshold level such that $\rho_I^2 = R_I^2/P_I$. $\sigma_{V_I}^2$ is the spatial fading rate variance of the WSS complex interference voltage, defined as [29]

$$\sigma_{V_I}^2(\varphi_0) = \mathbb{E}\left[\left|\frac{\mathrm{d}\left[V_I(l)\exp(-jk_c l)\right]}{\mathrm{d}l}\right|^2\right] \tag{9}$$

where l represents displacement of the receiver traveling along φ_0. The value of k_c is the centroid of the wavenumber spectrum calculated for the direction φ_0 as expressed in Appendix I-A in [29]. Applying the analogy between interference network and propagation channel, we can produce directly a concise expression of $\sigma_{V_I}^2$ by using the derived result in [29], which was obtained originally for the rate variance of complex received voltage in a directional propagation channel:

$$\sigma_{V_I}^2(\varphi_0) = \frac{2\pi^2 \Lambda_I^2 P_I}{\lambda^2} \left\{1 + \gamma_I \cos\left[2(\varphi_0 - \varphi_{I,\max})\right]\right\}. \tag{10}$$

In (10), λ is the wavelength of the carrier frequency

$$\Lambda_I = \sqrt{1 - \frac{|F_{I,1}|^2}{F_{I,0}^2}} \tag{11}$$

$$\gamma_I = \frac{\left|F_{I,0}F_{I,2} - F_{I,1}^2\right|}{F_{I,0}^2 - |F_{I,1}|^2} \tag{12}$$

$$\varphi_{I,\max} = \frac{1}{2}\arg\left(F_{I,0}F_{I,2} - F_{I,1}^2\right) \tag{13}$$

are the multipath shape factors introduced in [29], where

$$F_{I,n} = \int_0^{2\pi} \Xi_I^{(\mathrm{IAS})}(\varphi) G(\varphi) \exp(jn\varphi) \mathrm{d}\varphi \tag{14}$$

is the nth Fourier coefficient of $\Xi_I^{(\mathrm{IAS})}(\varphi)G(\varphi)$. The physical meanings of these shape factors in an interference network can be understood in a similar way to those in a multipath propagation channel as elaborated in [29]. The shape factor Λ_I in (11) is a measure of how interference signals concentrate about a single azimuthal direction. It ranges from 0 to 1, with 0 indicating the case of interference from a single direction and 1 indicating no clear bias in the angular distribution of interference. The shape factor γ_I in (12) is a measure of how interference signals concentrate about two azimuthal directions. It also ranges from 0 to 1, with 0 indicating no clear bias in two arrival directions and 1 indicating the case of exactly two interference signals from two different directions. Finally, the shape factor $\varphi_{I,\max}$ in (13) is the azimuthal direction of maximum interference fading. The term $G(\varphi)$ in (14) includes both antenna gain and polarization mismatch effects. Substituting (10) into (8) yields the LCR of the interference envelope process:

$$N_I(\rho_I) = \frac{\sqrt{2\pi}\Lambda_I \sqrt{1 + \gamma_I \cos\left[2(\varphi_0 - \varphi_{I,\max})\right]}}{\lambda} \frac{m_I^{m_I-1/2}}{\Gamma(m_I)} \times \rho_I^{2m_I-1} \exp\left(-m_I \rho_I^2\right). \tag{15}$$

2) LCR of SIR: Suppose that the PAS from the desired transmitter is $\Xi_S^{(\mathrm{PAS})}$ and its envelope also follows the Nakagami-m distribution. The LCR of the desired signal can be obtained in a similar way to (15):

$$N_S(\rho_S) = \frac{\sqrt{2\pi}\Lambda_S\sqrt{1+\gamma_S\cos\left[2(\varphi_0-\varphi_{S,\max})\right]}}{\lambda}\frac{m_S^{m_S-1/2}}{\Gamma(m_S)} \times \rho_S^{2m_S-1}\exp\left(-m_S\rho_S^2\right) \quad (16)$$

where the subscript S indicates desired signal throughout the paper and the multipath shape factors Λ_S, γ_S, and $\varphi_{S,\max}$ can be derived in a similar way to (11)–(13) by replacing $\Xi_I^{(\mathrm{IAS})}$ in (14) with $\Xi_S^{(\mathrm{PAS})}$.

Obtaining the LCR of SIR η requires the joint pdf, $f_{r_I,\dot{r}_I,r_S,\dot{r}_S}(r_I,\dot{r}_I,r_S,\dot{r}_S)$, of the envelope levels r_I, r_S, and the envelope slopes $\dot{r}_I$, $\dot{r}_S$, at any spatial position $l\hat{\mathbf{l}}$. The expected distance of traveling where the received interference and intended signal envelopes are in the intervals $(r_I, r_I+\mathrm{d}r_I)$ and $(r_S, r_S+\mathrm{d}r_S)$, respectively, for given envelope slopes $\dot{r}_I$, $\dot{r}_S$ and unit distance increment is

$$f_{r_I,\dot{r}_I,r_S,\dot{r}_S}(r_I,\dot{r}_I,r_S,\dot{r}_S)\mathrm{d}r_I\mathrm{d}\dot{r}_I\mathrm{d}r_S\mathrm{d}\dot{r}_S.$$

For each specific SIR threshold ρ_η, the following relationship should be satisfied: $r_S^2/r_I^2=\rho_\eta$.

In terms of interference, the distance traveled by a mobile receiver in a local area to cross the level r_I once for a given envelope slope $\dot{r}_I$, in the interval $(r_I, r_I+\mathrm{d}r_I)$ is $\mathrm{d}r_I/\dot{r}_I$. Similarly, in terms of desired signal, the distance traveled to cross the level r_S once for a given envelope slope $\dot{r}_S$, in the interval $(r_S, r_S+\mathrm{d}r_S)$ is $\mathrm{d}r_S/\dot{r}_S$. Subsequently, the expected number of downward crossings of the SIR threshold ρ_η for unit distance increment is calculated to be

$$\frac{f_{r_I,\dot{r}_I,r_S,\dot{r}_S}(r_I,\dot{r}_I,\sqrt{\rho_\eta}r_I,\dot{r}_S)\sqrt{\rho_\eta}\mathrm{d}r_I\mathrm{d}\dot{r}_I\mathrm{d}r_I\mathrm{d}\dot{r}_S}{\min\left\{\left|\frac{\mathrm{d}r_I}{\dot{r}_I}\right|,\left|\frac{\sqrt{\rho_\eta}\mathrm{d}r_I}{\dot{r}_S}\right|\right\}},\ \dot{r}_I>\dot{r}_S$$

and the LCR is obtained as

$$\begin{aligned}
&N_\eta(\rho_\eta)\\
&=\iiiint\limits_{\dot{r}_I>\dot{r}_S}\frac{f_{r_I,\dot{r}_I,r_S,\dot{r}_S}(r_I,\dot{r}_I,\sqrt{\rho_\eta}r_I,\dot{r}_S)\sqrt{\rho_\eta}}{\min\left\{\left|\frac{\mathrm{d}r_I}{\dot{r}_I}\right|,\left|\frac{\sqrt{\rho_\eta}\mathrm{d}r_I}{\dot{r}_S}\right|\right\}}\mathrm{d}r_I\mathrm{d}\dot{r}_I\mathrm{d}r_I\mathrm{d}\dot{r}_S\\
&=\iiint\limits_{\dot{r}_I>\dot{r}_S}\frac{f_{r_I,\dot{r}_I,r_S,\dot{r}_S}(r_I,\dot{r}_I,\sqrt{\rho_\eta}r_I,\dot{r}_S)\sqrt{\rho_\eta}}{\min\left\{\left|\frac{1}{\dot{r}_I}\right|,\left|\frac{\sqrt{\rho_\eta}}{\dot{r}_S}\right|\right\}}\mathrm{d}r_I\mathrm{d}\dot{r}_I\mathrm{d}\dot{r}_S\\
&\overset{(a)}{=}\int_0^\infty f_{r_I}(r_I)f_{r_S}(\sqrt{\rho_\eta}r_I)\mathrm{d}r_I\\
&\qquad\times\iint\limits_{\dot{r}_I>\dot{r}_S}\frac{f_{\dot{r}_I}(\dot{r}_I)f_{\dot{r}_S}(\dot{r}_S)\sqrt{\rho_\eta}}{\min\left\{\left|\frac{1}{\dot{r}_I}\right|,\left|\frac{\sqrt{\rho_\eta}}{\dot{r}_S}\right|\right\}}\mathrm{d}\dot{r}_I\mathrm{d}\dot{r}_S. \qquad (17)
\end{aligned}$$

The relationship (a) follows from the result that in the Nakagami-m case as in the Rayleigh and Rice cases, $\dot{r}$ and r are independent random variables [28], and makes use of the assumption that interference and intended signal channels are independent. We can further derive (17) as (18) (see equation at the bottom of the page). The distribution of r_I is given in (6). Similar Nakagami-m expression can be used to describe the random variable r_S. Moreover, the pdfs of $\dot{r}_I$ and $\dot{r}_S$ are Gaussian distributed with standard deviations $\sigma_{V_I}/\sqrt{2m_I}$ and $\sigma_{V_S}/\sqrt{2m_S}$, respectively [28]. Using these results in (18), we can obtain the LCR of SIR.

$$\begin{aligned}
N_\eta(\rho_\eta) &= \int_0^\infty f_{r_I}(r_I)f_{r_S}(\sqrt{\rho_\eta}r_I)\mathrm{d}r_I\times\int_{-\infty}^{\infty}\int_{-\infty}^{\dot{r}_I}\frac{f_{\dot{r}_I}(\dot{r}_I)f_{\dot{r}_S}(\dot{r}_S)\sqrt{\rho_\eta}}{\min\left\{\left|\frac{1}{\dot{r}_I}\right|,\left|\frac{\sqrt{\rho_\eta}}{\dot{r}_S}\right|\right\}}\mathrm{d}\dot{r}_S\mathrm{d}\dot{r}_I\\
&=\begin{cases}
\int_0^\infty f_{r_I}(r_I)f_{r_S}(\sqrt{\rho_\eta}r_I)\mathrm{d}r_I\\
\times\left[\int_{-\infty}^0 f_{\dot{r}_I}(\dot{r}_I)\int_{-\infty}^{\dot{r}_I}-\dot{r}_S f_{\dot{r}_S}(\dot{r}_S)\mathrm{d}\dot{r}_S\mathrm{d}\dot{r}_I\right.\\
\quad+\int_0^\infty f_{\dot{r}_I}(\dot{r}_I)\int_{-\infty}^{-\sqrt{\rho_\eta}\dot{r}_I}-\dot{r}_S f_{\dot{r}_S}(\dot{r}_S)\mathrm{d}\dot{r}_S\mathrm{d}\dot{r}_I+\int_0^\infty\sqrt{\rho_\eta}\dot{r}_I f_{\dot{r}_I}(\dot{r}_I)\int_{-\sqrt{\rho_\eta}\dot{r}_I}^{\sqrt{\rho_\eta}\dot{r}_I}f_{\dot{r}_S}(\dot{r}_S)\mathrm{d}\dot{r}_S\mathrm{d}\dot{r}_I\\
\quad\left.+\int_0^\infty f_{\dot{r}_I}(\dot{r}_I)\int_{\sqrt{\rho_\eta}\dot{r}_I}^{\dot{r}_I}\dot{r}_S f_{\dot{r}_S}(\dot{r}_S)\mathrm{d}\dot{r}_S\mathrm{d}\dot{r}_I\right], & \rho_\eta\in(0,1]\\
\int_0^\infty f_{r_I}(r_I)f_{r_S}(\sqrt{\rho_\eta}r_I)\mathrm{d}r_I\\
\times\left[\int_{-\infty}^0 f_{\dot{r}_I}(\dot{r}_I)\int_{-\infty}^{\sqrt{\rho_\eta}\dot{r}_I}-\dot{r}_S f_{\dot{r}_S}(\dot{r}_S)\mathrm{d}\dot{r}_S\mathrm{d}\dot{r}_I\right.\\
\quad+\int_{-\infty}^0-\sqrt{\rho_\eta}\dot{r}_I f_{\dot{r}_I}(\dot{r}_I)\int_{\sqrt{\rho_\eta}\dot{r}_I}^{\dot{r}_I}f_{\dot{r}_S}(\dot{r}_S)\mathrm{d}\dot{r}_S\mathrm{d}\dot{r}_I+\int_0^\infty f_{\dot{r}_I}(\dot{r}_I)\int_{-\infty}^{-\sqrt{\rho_\eta}\dot{r}_I}-\dot{r}_S f_{\dot{r}_S}(\dot{r}_S)\mathrm{d}\dot{r}_S\mathrm{d}\dot{r}_I\\
\quad\left.+\int_0^\infty\sqrt{\rho_\eta}\dot{r}_I f_{\dot{r}_I}(\dot{r}_I)\int_{-\sqrt{\rho_\eta}\dot{r}_I}^{\dot{r}_I}f_{\dot{r}_S}(\dot{r}_S)\mathrm{d}\dot{r}_S\mathrm{d}\dot{r}_I\right], & \rho_\eta\in(1,\infty)
\end{cases} \qquad (18)
\end{aligned}$$

If interference fading is much slower than desired signal fluctuation, i.e., $N_I(\rho_I=\rho,\varphi_0) \ll N_S(\rho_S=\rho,\varphi_0)$ for almost all ρ and φ_0, we can obtain an approximate expression of LCR. In this case, the interference remains at a certain level whereas the desired signal has experienced fast variation. The LCR of SIR can thus be approximated by the expected level crossing of the fast fading signal, N_S, averaged over the slow fading interference, r_I. The threshold ρ_S for N_S should be set to ensure that the overall SIR threshold is $\rho_\eta = \rho_S^2 P_S / r_I^2$. As a result, the LCR of SIR is given by

$$\begin{aligned} N_\eta(\rho_\eta) &\approx \int_0^\infty N_S\left(\rho_S = \sqrt{\frac{\rho_\eta r_I^2}{P_S}}\right) f_{r_I}(r_I)\mathrm{d}r_I \\ &\approx \int_0^\infty \frac{\sqrt{2\pi}\Lambda_S\sqrt{1+\gamma_S\cos\left[2(\varphi_0-\varphi_{S,\max})\right]}}{\lambda} \\ &\quad \times \frac{m_S^{m_S-1/2}}{\Gamma(m_S)}\left(\frac{\rho_\eta r_I^2}{P_S}\right)^{m_S-1/2}\exp\left(-\frac{m_S\rho_\eta r_I^2}{P_S}\right) \\ &\quad \times \frac{2m_I^{m_I} r_I^{2m_I-1}}{\Gamma(m_I)P_I^{m_I}}\exp\left(-\frac{m_I r_I^2}{P_I}\right)\mathrm{d}r_I. \end{aligned} \tag{19}$$

A careful examination of (18) reveals that, by setting $|1/\dot{r}_I| \gg |\sqrt{\rho_\eta}/\dot{r}_S| \approx 0$, we can obtain the expression of (19).

On the other hand, if interference fading is much faster than intended signal fading, i.e., $N_I(\rho_I=\rho,\varphi_0) \gg N_S(\rho_S=\rho,\varphi_0)$ for almost all ρ and φ_0, the LCR of SIR can be approximated by the expected level crossing of the fast fading interference, N_I, averaged over the slow fading signal, r_S. The threshold ρ_I for N_I is constrained by the relationship $\rho_\eta = r_S^2/(\rho_I^2 P_I)$. The LCR of SIR is obtained as

$$\begin{aligned} N_\eta(\rho_\eta) &\approx \int_0^\infty N_I\left(\rho_I = \sqrt{\frac{r_S^2}{\rho_\eta P_I}}\right) f_{r_S}(r_S)\mathrm{d}r_S \\ &\approx \int_0^\infty \frac{\sqrt{2\pi}\Lambda_I\sqrt{1+\gamma_I\cos\left[2(\varphi_0-\varphi_{I,\max})\right]}}{\lambda} \\ &\quad \times \frac{m_I^{m_I-1/2}}{\Gamma(m_I)}\left(\frac{r_S^2}{\rho_\eta P_I}\right)^{m_I-1/2}\exp\left(-\frac{m_I r_S^2}{\rho_\eta P_I}\right) \\ &\quad \times \frac{2m_S^{m_S} r_S^{2m_S-1}}{\Gamma(m_S)P_S^{m_S}}\exp\left(-\frac{m_S r_S^2}{P_S}\right)\mathrm{d}r_S. \end{aligned} \tag{20}$$

Similarly, by setting $|\sqrt{\rho_\eta}/\dot{r}_S| \gg |1/\dot{r}_I| \approx 0$ in (18), we can obtain the result in (20).

C. Fade Distance

1) AFD of Interference: The AFD is the traveling distance of a receiver in a local area, where the received interference envelope is underneath a threshold level, once the envelope has crossed that level. For a given threshold level $\rho_I = R_I^2/P_I$, the AFD, $\bar{l}_I$, is calculated by the following:

$$\bar{l}_I = \frac{1}{N_I(\rho_I)}\int_0^{R_I} f_{r_I}(r_I)\mathrm{d}r_I. \tag{21}$$

Substituting (15) and the Nakagami-m pdf in (6) into (21) yields

$$\begin{aligned} \bar{l}_I &= \frac{\lambda}{\sqrt{2\pi}\Lambda_I\sqrt{1+\gamma_I\cos\left[2(\varphi_0-\varphi_{I,\max})\right]}} \\ &\quad \times \frac{\hat{\gamma}(m_I, m_I\rho_I)}{m_I^{m_I-1/2}\rho_I^{2m_I-1}}\exp(m_I\rho_I^2) \end{aligned} \tag{22}$$

where $\hat{\gamma}(\cdot,\cdot)$ is the incomplete Gamma function.

2) AFD of SIR: Following (21), we can derive the AFD of SIR as:

$$\begin{aligned} \bar{l}_\eta &= \frac{1}{N_\eta(\rho_\eta)}\int_0^{\rho_\eta} f_\eta(\eta)\mathrm{d}\eta \\ &\overset{(a)}{=} \frac{1}{N_\eta(\rho_\eta)}\int_0^{\rho_\eta} \frac{\left(\frac{m_S P_I}{m_I P_S}\right)^{m_S}}{B(m_S,m_I)}\left(1+\frac{m_S P_I\eta}{m_I P_S}\right)^{-m_S-m_I} \\ &\quad \times \eta^{m_S-1}\mathrm{d}\eta \\ &\overset{(b)}{\geq} \frac{1}{N_\eta(\rho_\eta)}\left(1-\frac{\mathbb{E}[\eta]}{\rho_\eta}\right) \\ &= \frac{1}{N_\eta(\rho_\eta)}\left[1-\frac{\left(\frac{m_S P_I}{m_I P_S}\right)^{-1}\frac{\Gamma(m_S+1)}{\Gamma(m_S)}\frac{\Gamma(m_I-1)}{\Gamma(m_I)}}{\rho_\eta}\right] \end{aligned} \tag{23}$$

where $B(\cdot,\cdot)$ is the Beta function. (a) applies the fact that the ratio of two independent Gamma distributions is a generalized Gamma-ratio pdf and (b) follows from the Markov's inequality. Substituting (18), (19), or (20) into (23) yields a lower bound of the AFD of SIR. Note that when $P_I = P_S$, the generalized Gamma-ratio pdf reduces to the F-distribution and the AFD is expressed as

$$\begin{aligned} \bar{l}_\eta &= \frac{1}{N_\eta(\rho_\eta)}\int_0^{\rho_\eta} \frac{\left(\frac{m_S}{m_I}\right)^{m_S}}{B(m_S,m_I)}\left(1+\frac{m_S\eta}{m_I}\right)^{-m_S-m_I} \\ &\quad \times \eta^{m_S-1}\mathrm{d}\eta \\ &= \frac{1}{N_\eta(\rho_\eta)}\mathcal{I}_{\frac{m_S\rho_\eta}{m_S\rho_\eta+m_I}}(m_S,m_I) \end{aligned} \tag{24}$$

where $\mathcal{I}$ is the regularized incomplete Beta function.

D. Spatial Autocovariance

1) Autocovariance of Interference: The spatial autocovariance of received interference envelope is defined as the correlation of envelope as a function of change in receiver position.

This quantity is useful if we want to study spatial diversity to combat spatial selectivity in *interference networks* (analogous to its counterpart in propagation channels), where we attempt to reduce the overall interference level by using multiple antennas physically separated from one another. This arrangement offers a receiver several observations of the same signal. Thus, if one antenna is experiencing a severe interference, it is likely that another has a deep fade (hence potentially higher SIR). Collectively such a system can provide a robust link.

The autocovariance function of the interfering signal envelope is defined as follows:

$$\varrho_I(l) = \frac{\mathbb{E}\left[r_I\{\mathbf{l}_0\} r_I\{\mathbf{l}_0 + l\hat{\mathbf{l}}\}\right] - \mathbb{E}^2[r_I]}{\mathbb{E}\left[r_I^2\right] - \mathbb{E}^2[r_I]} \tag{25}$$

where $\mathbf{l}_0$ is the reference position in the azimuthal plane and is arbitrary if the fading process is WSS. $\hat{\mathbf{l}}$ is a unit vector pointing in the direction of traveling, φ_0. The Mclaurin series expansion of an autocovariance function is expressed as [30]

$$\begin{aligned}\varrho_I(l) &= 1 + \frac{\sum_{n=1}^{\infty} \frac{(-1)^n l^{2n}}{(2n)!} \mathbb{E}\left[\left(\frac{\mathrm{d}^n r_I}{\mathrm{d}l^n}\right)^2\right]}{\mathbb{E}\left[r_I^2\right] - \mathbb{E}^2[r_I]} \\ &= 1 - \frac{\mathbb{E}\left[\left(\frac{\mathrm{d}r_I}{\mathrm{d}l}\right)^2\right]}{2\left(\mathbb{E}\left[r_I^2\right] - \mathbb{E}^2[r_I]\right)} l^2 + \cdots \\ &= 1 - \frac{2\pi^2 \Lambda_I^2 \left\{1 + \gamma_I \cos\left[2(\varphi_0 - \varphi_{I,\max})\right]\right\}}{\lambda^2 \left\{1 - \frac{1}{m_I}\left[\frac{\Gamma(m_I + 1/2)}{\Gamma(m_I)}\right]^2\right\}} l^2 + \cdots . \end{aligned} \tag{26}$$

Following the approach in [29], suppose that $\varrho_I(l)$ is approximated by an arbitrary Gaussian function and its Mclaurin expansion is

$$\begin{aligned}\varrho_I(l) &\approx \exp\left[-\nu_I \left(\frac{l}{\lambda}\right)^2\right] \\ &\approx 1 - \nu_I \left(\frac{l}{\lambda}\right)^2 + \cdots . \end{aligned} \tag{27}$$

A Gaussian function is chosen as a generic approximation to the true autocovariance since it is a convenient and well-behaved correlation function. This approximation is nearly exact for values of l less than or equal to the correlation distance of interference $l_{I,c}$, defined as the value that satisfies the relationship $\varrho_I(l_{I,c}) = 0.5$[29]. The appropriate constant ν_I is selected such that the second terms of (26) and (27) are equal, ensuring that the behavior of both autocovariance functions are identical for small l

$$\nu_I = \frac{2\pi^2 \Lambda_I^2 \left\{1 + \gamma_I \cos\left[2(\varphi_0 - \varphi_{I,\max})\right]\right\}}{1 - \frac{1}{m_I}\left[\frac{\Gamma(m_I + 1/2)}{\Gamma(m_I)}\right]^2}. \tag{28}$$

Using the autocovariance function of (27) leads to

$$l_{I,c} = \frac{\lambda\sqrt{\ln 2}\sqrt{1 - \frac{1}{m_I}\left[\frac{\Gamma(m_I + 1/2)}{\Gamma(m_I)}\right]^2}}{\sqrt{2}\pi\Lambda_I\sqrt{1 + \gamma_I \cos\left[2(\varphi_0 - \varphi_{I,\max})\right]}}. \tag{29}$$

2) Autocovariance of SIR: A more explicit measure for studies in spatial diversity is the autocovariance of SIR, which is directly related to the achievable rate of the system. Following (25), we have

$$\begin{aligned}\mathbb{E}\left[\Theta_I(l)\right] &= \mathbb{E}\left[r_I\{\mathbf{l}_0\} r_I\{\mathbf{l}_0 + l\hat{\mathbf{l}}\}\right] \\ &= \varrho_I(l)\left(\mathbb{E}\left[r_I^2\right] - \mathbb{E}^2[r_I]\right) + \mathbb{E}^2[r_I] \\ &= \exp\left[-\nu_I \left(\frac{l}{\lambda}\right)^2\right]\left\{P_I - \frac{P_I}{m_I}\left[\frac{\Gamma(m_I + 1/2)}{\Gamma(m_I)}\right]^2\right\} \\ &\quad + \frac{P_I}{m_I}\left[\frac{\Gamma(m_I + 1/2)}{\Gamma(m_I)}\right]^2 . \end{aligned} \tag{30}$$

In a similar way, we can derive $\mathbb{E}[\Theta_S(l)] = \mathbb{E}[r_S\{\mathbf{l}_0\} r_S\{\mathbf{l}_0 + l\hat{\mathbf{l}}\}]$ for the desired signal channel.

Suppose that the function $\Theta_\eta(l) = \eta\{\mathbf{l}_0\}\eta\{\mathbf{l}_0 + l\hat{\mathbf{l}}\} = (r_S^2\{\mathbf{l}_0\} / r_I^2\{\mathbf{l}_0\}) \times (r_S^2\{\mathbf{l}_0 + l\hat{\mathbf{l}}\} / r_I^2\{\mathbf{l}_0 + l\hat{\mathbf{l}}\}) = ([\Theta_S(l)]^2 / [\Theta_I(l)]^2)$ is sufficiently smooth near the point $(\mathbb{E}[\Theta_I(l)], \mathbb{E}[\Theta_S(l)])$ and the interference and intended signal channels are uncorrelated, then the mean $\mathbb{E}[\Theta_\eta(l)]$ can be estimated in terms of the mean and variance of $\Theta_I(l)$ and $\Theta_S(l)$ [30]

$$\begin{aligned}&\mathbb{E}\left[\Theta_\eta(l)\right] \\ &\quad \approx \frac{\mathbb{E}^2\left[\Theta_S(l)\right]}{\mathbb{E}^2\left[\Theta_I(l)\right]} + \frac{1}{2}\left[\frac{\partial^2 \Theta_\eta(l)}{\partial \Theta_I^2(l)} \sigma^2_{\Theta_I(l)} + \frac{\partial^2 \Theta_\eta(l)}{\partial \Theta_S^2(l)} \sigma^2_{\Theta_S(l)}\right] \\ &\quad = \frac{\mathbb{E}^2\left[\Theta_S(l)\right]}{\mathbb{E}^2\left[\Theta_I(l)\right]} + \frac{1}{2}\left[\frac{6\mathbb{E}^2\left[\Theta_S(l)\right]}{\mathbb{E}^4\left[\Theta_I(l)\right]} \sigma^2_{\Theta_I(l)} + \frac{2}{\mathbb{E}^2\left[\Theta_I(l)\right]} \sigma^2_{\Theta_S(l)}\right] \\ &\quad \approx \frac{\mathbb{E}^2\left\{\Theta_S(l)\right\}}{\mathbb{E}^2\left[\Theta_I(l)\right]} \\ &\qquad + \frac{1}{2}\left[\frac{6\mathbb{E}^2\left\{\Theta_S(l)\right\}}{\mathbb{E}^4\left[\Theta_I(l)\right]} \sigma^2_{\Theta_I(0)} + \frac{2}{\mathbb{E}^2\left[\Theta_I(l)\right]} \sigma^2_{\Theta_S(0)}\right]. \end{aligned} \tag{31}$$

Next, the variance of $\Theta_I(l)$ and $\Theta_S(l)$ at $l = 0$ are given by

$$\sigma^2_{\Theta_I(0)} = \mathbb{E}\left[r_I^4\right] - \mathbb{E}^2\left[r_I^2\right] = \frac{P_I^2}{m_I} \tag{32}$$

and

$$\sigma^2_{\Theta_S(0)} = \mathbb{E}\left[r_S^4\right] - \mathbb{E}^2\left[r_S^2\right] = \frac{P_S^2}{m_S} \tag{33}$$

respectively. Substituting (30), (32), and (33) into (31) yields the approximate expression of $\mathbb{E}[\Theta_\eta(l)]$. Hence, the autocovariance of the SIR is computed as

$$\varrho_\eta(l) = \frac{\mathbb{E}\left[\Theta_\eta(l)\right] - \mathbb{E}^2[\eta]}{\mathbb{E}[\eta^2] - \mathbb{E}^2[\eta]}. \tag{34}$$

Applying (31) in (34) and noting that for the Generalized Gamma-ratio pdf, the hth moment is derived as

$$\mathbb{E}[\eta^h] = \left(\frac{m_S P_I}{m_I P_S}\right)^{-h} \frac{\Gamma(m_S + h)}{\Gamma(m_S)} \frac{\Gamma(m_I - h)}{\Gamma(m_I)} \tag{35}$$

we can readily obtain $\varrho_\eta(l)$.

IV. Azimuthal Spectrum of Achievable Rate and Outage Analysis

A. Azimuthal Spectrum of Average Rate

Modern wireless networks often employ link-adaptive algorithms, which allow the average SIR to be explicitly related to the average data rate. Suppose that adaptive modulation and coding is applied. We define the expected achievable rate of a link based upon the Shannon capacity expression, $\mathbb{E}[\ln(1+\eta)]$, averaging over the random SIR.

Suppose that the receiver antenna boresight points towards the direction $\varphi_{\rm b}$ and therefore, its antenna beampattern can be expressed as $G(\varphi-\varphi_{\rm b})$. As the mean of $\ln(1+\eta)$ can be interpreted as a Lebesgue integral, the corresponding average data rate can be derived as

$$\begin{aligned}\mathcal{R}_{\rm avg}(\varphi_{\rm b}) &= \mathbb{E}\left[\ln(1+\eta)\right] \\ &= \int_s \ln(1+\eta)\mathrm{d}P \\ &= \int_\eta \ln(1+\eta) f_\eta(\eta)\mathrm{d}\eta \\ &= \int_\eta \ln(1+\eta)\frac{\left[\frac{m_S\tilde{\Xi}_I^{(\rm IAS)}(\varphi_{\rm b})}{m_I\tilde{\Xi}_S^{(\rm PAS)}(\varphi_{\rm b})}\right]^{m_S}}{B(m_S,m_I)} \\ &\quad\times\left[1+\frac{m_S\tilde{\Xi}_I^{(\rm IAS)}(\varphi_{\rm b})\eta}{m_I\tilde{\Xi}_S^{(\rm PAS)}(\varphi_{\rm b})}\right]^{-m_S-m_I}\eta^{m_S-1}\mathrm{d}\eta. \quad (36)\end{aligned}$$

In (36), the mean received interference and signal powers, defined as the antenna-dependent *effective* IAS and PAS, are given by

$$\tilde{\Xi}_I^{(\rm IAS)}(\varphi_{\rm b}) = \int_0^{2\pi}\Xi_I^{(\rm IAS)}(\varphi)G(\varphi-\varphi_{\rm b})\mathrm{d}\varphi \quad (37)$$

and

$$\tilde{\Xi}_S^{(\rm PAS)}(\varphi_{\rm b}) = \int_0^{2\pi}\Xi_S^{(\rm PAS)}(\varphi)G(\varphi-\varphi_{\rm b})\mathrm{d}\varphi \quad (38)$$

respectively.

We define the quantity $\mathcal{R}_{\rm avg}(\varphi_{\rm b})$ to be the ARAS in this work. Note that in the limiting case when a pencil-beam antenna is employed, i.e., $G(\varphi-\varphi_{\rm b})\approx\delta(\varphi-\varphi_{\rm b})$, (37) and (38) reduce to

$$\tilde{\Xi}_I^{(\rm IAS)}(\varphi_{\rm b}) = \Xi_I^{(\rm IAS)}(\varphi_{\rm b}) \quad (39)$$

and

$$\tilde{\Xi}_S^{(\rm PAS)}(\varphi_{\rm b}) = \Xi_S^{(\rm PAS)}(\varphi_{\rm b}) \quad (40)$$

respectively.

B. Local Area Outage and FZI in a Global Area

Consider that a receiver travels within a local area, where the angular statistics of both interference and desired signal remain unchanged. If the pdf of the receive antenna boreshight can be expressed as $f_{\varphi_{\rm b}}(\varphi_{\rm b})$, we may define the outage average rate in a local area to be

$$\mathcal{R}_{\rm avg}^{(\epsilon)} \triangleq \sup\left\{\hat{\mathcal{R}}_{\rm avg}\in[\mathcal{R}_{\min},\mathcal{R}_{\max}] : \Pr\{\mathcal{R}_{\rm avg}\le\hat{\mathcal{R}}_{\rm avg}\}<\epsilon\right\} \quad (41)$$

where ϵ is the outage probability measure, and $\mathcal{R}_{\min}$ and $\mathcal{R}_{\max}$ are the minimum and maximum average rates, respectively. This quantity defines the supremum limit of the average rate such that the probability of observing a smaller value of ARAS at a random $\varphi_{\rm b}$ is less than ϵ.

In the special case that $\mathcal{R}_{\rm avg}(\varphi_{\rm b})$ has a symmetric shape with respect to the mean azimuth $\varphi_{\rm b,0}$, where the peak rate is achieved, and $\mathcal{R}_{\rm avg}(\varphi_{\rm b})$ decreases monotonically as $|\varphi_{\rm b}-\varphi_{\rm b,0}|$ increases, (41) can be simplified as

$$\mathcal{R}_{\rm avg}^{(\epsilon)} = \mathcal{R}_{\rm avg}(\varphi_{\rm b,0}\pm\Delta\varphi_{\rm b}) \quad (42)$$

where $\Delta\varphi_{\rm b}$ is the solution to the following equation $\int_{\varphi_{\rm b,0}-\Delta\varphi_{\rm b}}^{\varphi_{\rm b,0}+\Delta\varphi_{\rm b}} f_{\varphi_{\rm b}}(\varphi_{\rm b})\mathrm{d}\varphi_{\rm b}=\epsilon$.

Consequently, we may define the FZI in a global service area to be

$$\mathbb{Z}_\vartheta \triangleq \left\{(x,y) : \mathcal{R}_{\rm avg}^{(\epsilon)}(x,y)\le\vartheta\right\} \quad (43)$$

where ϑ is a sufficiently large outage average rate and (x,y) are the Cartesian coordinates of the receiver location.

V. Geometric Modeling of Interference Networks

In this section, we elaborate on the geometric modeling of interference networks, similar to the classical GBSM setup in propagation channels (see e.g., [16], [31]–[34]), where interfering terminals are randomly located according to a specified spatial density function. This approach stochastically characterizes the spatial properties of interference networks with a small set of parameters. For a large number of interferers, the GBSM is equivalent to a continuum network, where the network area is kept fixed and the number of interferers approaches infinity.

Implementation of the GBSM for an interference network involves the following steps. A pictorial illustration is provided in Fig. 3.

1) Assign random locations to the centers of interfering clusters in the service area according to a pre-specified clustering scenario. This aggregation of interfering terminals in space may be due to geographical factors (e.g., interference from regions with multiple random hotspots, out-of-cell interference in cellular networks with user clustering or in two-tier femtocell networks, etc.) or MAC layer protocols [2]. No interferer is allowed to be collocated with the receiver to avoid infinite interference power. This is not an issue from the model implementation point-of-view, as the probability of generating an interferer

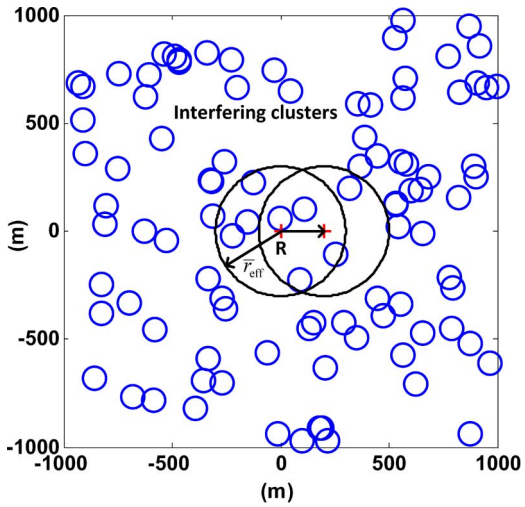

Fig. 3. Principles of the GBSM to include temporal variation of interfering clusters.

whose location is exactly the same as that of the receiver is 0. Note that interferer clustering is not a necessary condition for the establishment of the analogy between propagation channels and interference networks, as well as the application of GBSM. Indeed, the multi-cluster model presented here represents a generalized network scenario, which includes the non-clustered situation as a special case when the number of clusters reduces to 1.

2) For each cluster, define its geometry and assign random locations to the intra-cluster interferers according to the distribution of their positions. The geometrical features (e.g., circular, annular, elliptical) categorize the average behavior over many spatial realizations of a *typical* network with irregularly scattered, densely populated nodes. For example, the annular distribution of interferers around the receiver $\mathbf{R}$ may be applicable to the situations where contention- or scheduling-based MAC protocols (or other local coordination techniques) are used to limit the interference, thereby creating a guard zone around $\mathbf{R}$ [2].
3) Implement the time-variant scenario when $\mathbf{R}$ moves. One possible way is to utilize all interfering radios to obtain the directional profile of interference. Otherwise, only those radios close to $\mathbf{R}$ are utilized to analyze the interference properties. Fig. 3 demonstrates one such example, where we consider only the interfering clusters distributed inside a circle of radius $\bar{r}_{\text{eff}}$ centered at $\mathbf{R}$ to be effective. The circular model has the physical interpretation that interference paths with larger propagation distances will incur more severe power loss and therefore do not make significant contributions. When $\mathbf{R}$ moves, so too does the circular disc. A number of new clusters contribute to the received interference by moving into the disc and at the same time, some clusters move out of the disc.
4) Given the effective interfering clusters and their respective geometries, determine the contributions of the effective nodes to the azimuthal statistics of interference and other related quantities presented in the earlier sections.

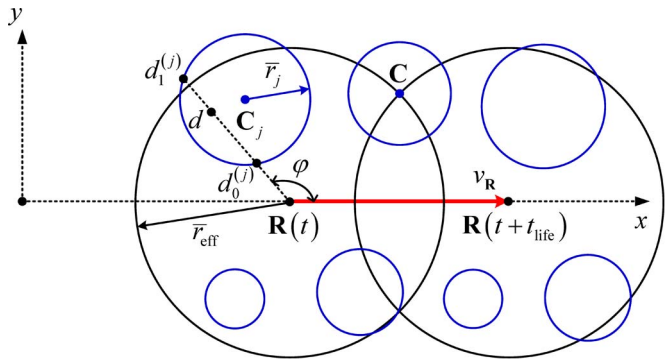

Fig. 4. Geometry for derivation of key GBSM parameters.

GBSMs have advantages when movement is to be simulated. Whenever the receiver moves, adjustments to the parameters of paths are made automatically. The motions of interfering terminals can also be easily incorporated in the models. Moreover, GBSMs often lead to trackable solutions for the properties of average network interference metrics when the number of realizations approaches infinity. In the following, we present the derivations of several key model parameters.

A. Derivations of Key GBSM Parameters

1) Number of Effective Interfering Clusters: The spatial Poisson point process is applied widely to the node placement of wireless networks [14], [35]. We can also apply the approximation here for the centers of interfering clusters. Suppose that W cluster centers are randomly deployed within an arbitrarily shaped region with an area A, the density of cluster centers is given by W/A. A cluster will become "effective" if its center $\mathbf{C}$ locates within the effective circular disc $\mathcal{D}_{\text{eff}}$ of area $A_{\text{eff}} = \pi\bar{r}_{\text{eff}}^2$. With Poisson node distribution, the probability mass function of w interfering clusters existing in $\mathcal{D}_{\text{eff}}$, where the contributions of interferers are taken into account, is

$$\Phi(w) = \frac{\exp\left(-\frac{WA_{\text{eff}}}{A}\right)\left(\frac{WA_{\text{eff}}}{A}\right)^w}{w!}. \tag{44}$$

2) Lifespan of Effective Interfering Clusters: As the receiver moves, some interfering clusters move out of the circular disc if their contributions to the received interference fall below some predetermined threshold while others move in. As a result, effective clusters exit for a period of time t_{life} and then disappear. Let the $x-y$ coordinate system be defined such that the receiver $\mathbf{R}$ lies on the x axis, as shown in Fig. 4. Suppose that the velocity of $\mathbf{R}$ in Fig. 4 is $v_{\mathbf{R}}$, whose footprint aligns with the x axis. An interfering cluster will be effective if the distance of its center, $\mathbf{C}$, to $\mathbf{R}$ is no greater than $\bar{r}_{\text{eff}}$. Following the geometry in Fig. 4, the lifespan of $\mathbf{C}$, t_{life}, actually corresponds to the time duration when $\mathbf{R}$ moves from $\mathbf{R}(t)$ to $\mathbf{R}(t+t_{\text{life}})$, both of which introduce the same distance to $\mathbf{C}$, which is $\bar{r}_{\text{eff}}$. Applying the basic trigonometry in Fig. 4 yields the distance between $\mathbf{R}(t)$ and $\mathbf{R}(t+t_{\text{life}})$, given as $2\sqrt{\bar{r}_{\text{eff}}^2 - y^2}$. The lifetime of the corresponding cluster is thus given by $t_{\text{life}} = 2\sqrt{\bar{r}_{\text{eff}}^2 - y^2}/v_{\mathbf{R}}$. We can then derive the

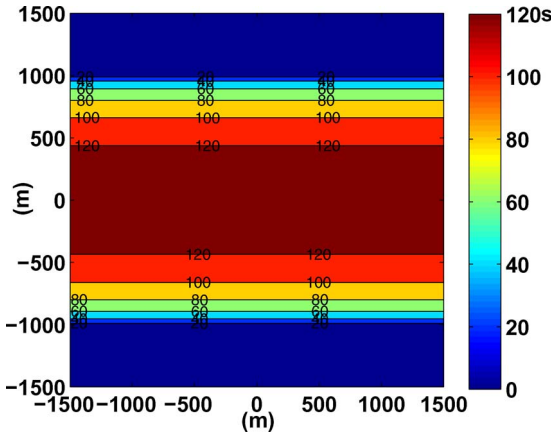

Fig. 5. Contours of the interfering cluster's lifetime. The radius of the circular disc of effective interfering clusters is set to be 1 km and the receiver travels along the x-axis at a velocity of 15 m/s.

cumulative distribution function (cdf) of t_{life} by applying the general formulation in [30]

$$F_{t_{\text{life}}}(t_{\text{life}}) = \iint\limits_{|y|\geq\sqrt{\bar{r}_{\text{eff}}^2 - v_{\mathbf{R}}^2 t_{\text{life}}^2/4}} f_{x_{\mathbf{C}},y_{\mathbf{C}}}(x,y)\mathrm{d}x\mathrm{d}y \tag{45}$$

where the integration domain represents the region in which the inequality $2\sqrt{\bar{r}_{\text{eff}}^2 - y^2}/v_{\mathbf{R}} \leq t_{\text{life}}$ is satisfied and $f_{x_{\mathbf{C}},y_{\mathbf{C}}}(x,y)$ is the pdf of cluster centers in the entire interference network. We can also calculate the average lifespan by integrating over the entire interference region to be

$$\begin{aligned}\mathbb{E}[t_{\text{life}}] &= \iint t_{\text{life}}(x,y) f_{x_{\mathbf{C}},y_{\mathbf{C}}}(x,y)\mathrm{d}x\mathrm{d}y \\ &= \iint \frac{2\sqrt{\bar{r}_{\text{eff}}^2 - y^2}}{v_{\mathbf{R}}} f_{x_{\mathbf{C}},y_{\mathbf{C}}}(x,y)\mathrm{d}x\mathrm{d}y. \end{aligned}\tag{46}$$

Fig. 5 illustrates the lifespan of interfering clusters when the radius of the effective circular disc is $\bar{r}_{\text{eff}} = 1$ km and the mobile receiver is traveling along the x-axis at a velocity of 15 m/s. These contours essentially define the integration region in (45) for different values of t_{life}. It can be seen from Fig. 5 that the farther the cluster centers from the receiver trajectory, the smaller their lifespan. Beyond certain distance, the time duration of interfering clusters reduces to zero. In other words, these clusters would never become effective contributors of interference at the receiver.

3) IAS in Clustered Interference Network: The geometry of a circular interfering cluster is shown in Fig. 4, which assumes that the interfering terminals are uniformly distributed within a radius $\bar{r}_j$ about the jth cluster center, $\mathbf{C}_j$.

The joint pdf $f_{d,\varphi}^{(j)}(d,\varphi)$ in the polar coordinates (d,φ) for cluster j is found using

$$f_{d,\varphi}^{(j)}(d,\varphi) = \left.\frac{f_{x_{\mathbf{I}},y_{\mathbf{I}}}^{(j)}(x,y)}{|\mathfrak{J}(x,y)|}\right|_{x=d\cos\varphi,\ y=d\sin\varphi} \tag{47}$$

where $\mathfrak{J}(x,y)$ is the Jacobian transformation given by

$$\begin{aligned}\mathfrak{J}(x,y) &= \begin{vmatrix} \frac{\partial x}{\partial d} & \frac{\partial x}{\partial \varphi} \\ \frac{\partial y}{\partial d} & \frac{\partial y}{\partial \varphi} \end{vmatrix}^{-1} \\ &= \begin{vmatrix} \cos\varphi & -d\sin\varphi \\ \sin\varphi & d\cos\varphi \end{vmatrix}^{-1} = \frac{1}{d} \end{aligned}\tag{48}$$

and $f_{x_{\mathbf{I}},y_{\mathbf{I}}}^{(j)}(x,y)$ is the joint pdf in the Cartesian coordinates for cluster j. Substituting (48) into (47) gives

$$f_{d,\varphi}^{(j)}(d,\varphi) = d f_{x_{\mathbf{I}},y_{\mathbf{I}}}^{(j)}(d\cos\varphi, d\sin\varphi). \tag{49}$$

For uniformly distributed interferers, we have

$$f_{d,\varphi}^{(j)}(d,\varphi) = \frac{d}{\sum_{j=1}^{J}\pi\bar{r}_j^2} \tag{50}$$

where J is the total number of clusters.

Following (3) and assuming that the transmission time of an interferer, τ', is i.i.d., the IAS due to the jth cluster is computed as

$$\begin{aligned}\Xi_I^{(j)}(\varphi) &\propto \int_{d_0^{(j)}(\varphi)}^{d_1^{(j)}(\varphi)} \int_0^{\infty} \mathbb{E}\left[|h_I|^2|\tau',d,\varphi\right] f_{\tau',d,\varphi}^{(j)}(\tau',d,\varphi)\mathrm{d}\tau'\mathrm{d}d \\ &= \int_{d_0^{(j)}(\varphi)}^{d_1^{(j)}(\varphi)} \mathbb{E}\left[|h_I|^2|d,\varphi\right] f_{d,\varphi}^{(j)}(d,\varphi)\mathrm{d}d \int_0^{\infty} f_{\tau'}^{(j)}(\tau')\mathrm{d}\tau' \\ &= \int_{d_0^{(j)}(\varphi)}^{d_1^{(j)}(\varphi)} \mathbb{E}\left[|h_I|^2|d,\varphi\right] f_{d,\varphi}^{(j)}(d,\varphi)\mathrm{d}d \end{aligned}\tag{51}$$

where $d_0^{(j)}(\varphi)$ and $d_1^{(j)}(\varphi)$ are the lower and upper integration limits at angle φ as illustrated in Fig. 4. These two limits are given as

$$\begin{aligned}d_0^{(j)}(\varphi), d_1^{(j)}(\varphi) = |\mathbf{RC}_j|\cos\left(\varphi - \varphi_{\mathbf{RC}_j}\right) \\ \mp\sqrt{\bar{r}_j^2 - |\mathbf{RC}_j|^2\sin^2\left(\varphi - \varphi_{\mathbf{RC}_j}\right)}. \end{aligned}\tag{52}$$

In (52), $|\mathbf{RC}_j|$ and $\varphi_{\mathbf{RC}_j}$ are the magnitude and angle of the vector $\mathbf{RC}_j$, respectively. The expected interference power conditioned on d and φ is given by

$$\mathbb{E}\left[|h_I|^2|d,\varphi\right] \propto d^{-n_{\text{PL}}}. \tag{53}$$

Substituting (50), (52), and (53) into (51) and taking into account the contributions from all interfering clusters yield

$$\begin{aligned}\Xi_I^{(\text{IAS})}(\varphi) &= \kappa\sum_{j=1}^{J}\Xi_I^{(j)}(\varphi) \\ &= \kappa\sum_{j=1}^{J}\int_{d_0^{(j)}(\varphi)}^{d_1^{(j)}(\varphi)} \frac{d^{1-n_{\text{PL}}}}{\sum_{j=1}^{J}\pi\bar{r}_j^2}\mathrm{d}d \end{aligned}\tag{54}$$

with κ being a normalization constant to ensure that $\int_{\varphi}\Xi_I^{(\text{IAS})}(\varphi) = 1$. The two terms $d_0^{(j)}(\varphi)$ and $d_1^{(j)}(\varphi)$ are given in (52).

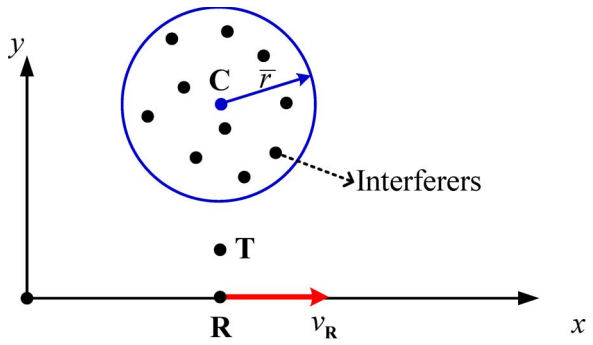

Fig. 6. Pictorial illustration of the simulation setting. The coordinates of the cluster center, the transmitter, and the starting location of the receiver are **C** (200 m, 200 m), **T** (200 m, 50 m), and **R** (200 m, 0 m), respectively. The radius of the interference cluster is $\bar{r} = 100$ m. The velocity of the receiver is $v_{\mathrm{R}} = 15$ m/s.

VI. Numerical Examples

We present numerical examples of characterizing wireless network interference in the angular domain with the proposed methodology. As shown in Fig. 6, we consider the scenario of a single interfering cluster, whose center **C** is located at (200 m,200 m). The radius of the cluster is $\bar{r} = 100$ m. The receiver **R** starts from the position (200 m, 0 m) and moves along the positive x-axis with a velocity of $v_{\mathbf{R}} = 15$ m/s. It is worth emphasizing that as **R** moves away from the interference cluster, the ratio of the cluster radius $\bar{r}$ to the distance between the cluster center and the receiver $|\mathbf{CR}|$ reduces. Hence, the study cases essentially investigate the effect of $\bar{r}/|\mathbf{CR}|$, which is a fundamental network geometric parameter in a circular GBSM [34], [36], on the interference behavior. The intended transmitter **T** is located at (200 m, 50 m). It is assumed that **T** introduces a Gaussian PAS at **R** with a standard deviation of 10°, which is fixed throughout the entire simulation process. Furthermore, the antenna beampattern at the receiver **R** is modeled using the Von Mises function $G(\varphi) = C\exp[2\cos(\varphi - \varphi_{\mathbf{RT}})]$ where C is a normalization constant, and the direction of maximum directive gain points towards the intended transmitter **T**. The system carrier frequency is set to be 1.8 GHz and the path loss exponent is $n_{\mathrm{PL}} = -2$. Finally, the Nakagami shape factors are set to be $m_I = m_S = 2$ for the interference and intended signal, respectively. Note that we are mainly concerned with the average properties of the network, which are applicable to the case that the number of spatial realizations of interferers approaches infinity, similar to the assumption made in any other statistical models [1]–[8].

Based on the analysis in Section V-A3, Fig. 7 shows the IAS and PAS observed at **R** after it travels for 0, 10, 20, and 30 seconds, which correspond to the Cartesian coordinates of (200 m, 0 m), (350 m, 0 m), (500 m, 0 m), and (650 m, 0 m), respectively. The following important observations can be made. Firstly, as **R** moves farther away from the interfering cluster, the IAS is confined within a narrower angular range around the mean AOA, where the maximum interference occurs. Furthermore, the shape of the IAS is very different from the traditional Gaussian or Laplacian distribution typically encountered in a PAS. Finally, the profiles of PAS often do not "match" those of IAS (e.g., their peak directions are not aligned

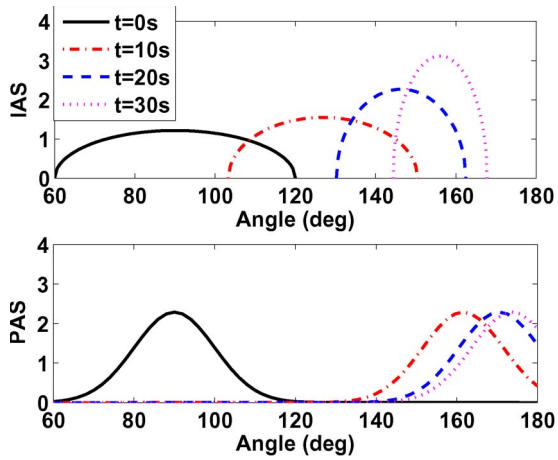

Fig. 7. IAS and PAS obtained at the receiver **R** after it travels for 0, 10, 20, and 30 seconds.

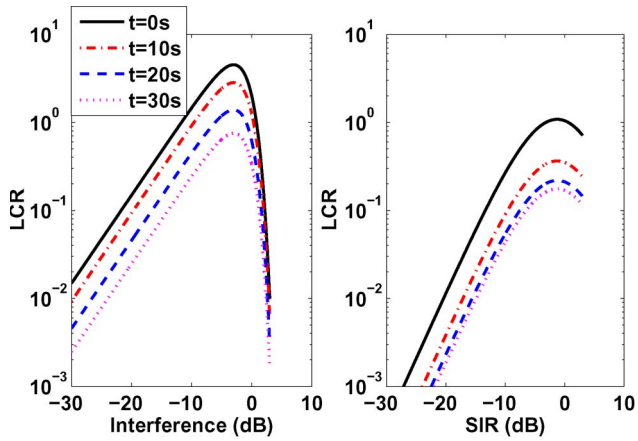

Fig. 8. LCRs of normalized interference and SIR obtained at the receiver **R** after it travels for 0, 10, 20, and 30 seconds.

at $t = 10, 20, 30$ s). As a result, we may expect much more complicated SIR-related performance measures in the angular domain as to be seen in Fig. 11.

Fig. 8 illustrates the LCRs of the normalized interference ρ_I and SIR ρ_η following the derivations in Section III-B1 and B2. In both cases, the maximum crossing rates are achieved when ρ_I and ρ_η are around 0 dB, and the crossing rates decrease as ρ_I and ρ_η deviate from 0 dB. This phenomenon shows that, when level crossing threshold is set to be either much higher or much lower than the mean value of interference or SIR, crossing becomes less probable. This is valid for the probability distributions commonly used in wireless propagation modeling and also agrees well with the classical LCR characteristics for fast fading signals. Moreover, the LCR of interference reduces at a much slower speed as compared to that of SIR for threshold values less than 0 dB, whereas an opposite trend can be noticed when the threshold values are greater than 0 dB. Finally, as the receiver moves farther away from the interfering cluster and the signal source, the LCRs decrease for both interference and SIR.

The AFDs of ρ_I and ρ_η are depicted in Fig. 9. Similar to the traditional AFD of desired signals, the AFDs of both interference and SIR increase with the threshold levels. Nevertheless, the AFD of interference exhibits a more apparent turning point

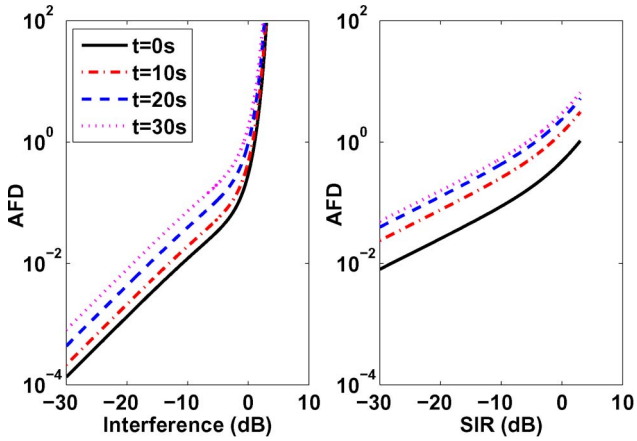

Fig. 9. AFDs of normalized interference and SIR obtained at the receiver $\mathbf{R}$ after it travels for 0, 10, 20, and 30 seconds.

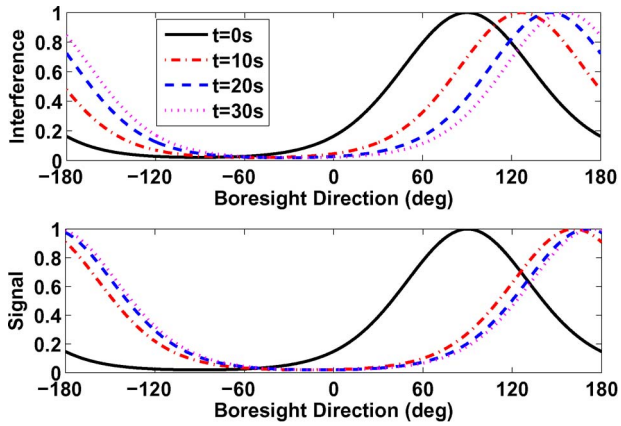

Fig. 10. Effective IAS and PAS (normalized with respect to the maximum values) obtained at the receiver $\mathbf{R}$ after it travels for 0, 10, 20, and 30 s.

near $\rho_I = 0$ dB, above which a much steeper slope is clearly visible. This phenomenon can be easily explained by observing the formulation of AFD in (21) and the LCR curves in Fig. 8 (left plot). As can be seen from this figure, for a normalized interference threshold above 0 dB, the LCR begins to decrease. Because the AFD in (21) is inversely proportional to the LCR, the AFD will begin to increase at a faster rate as compared to the case that the threshold is below 0 dB. On the other hand, the AFD of SIR increases at a gentler rate over the entire range of SIRs. This is due to the fact that the LCR of interference reduces at a much faster speed as compared to that of SIR for threshold values greater than 0 dB.

Finally, we focus upon the average date rate in the angular domain based on the results in Section IV. Fig. 10 shows the effective IAS and PAS normalized with respect to their maximum values at different traveling times (or equivalently, receiver locations). Similar to Fig. 7, except for the initial receiver location, the profiles of effective IAS do not "match" those of effective PAS, which also explains the ARAS shown in Fig. 11. At the initial location, the average achievable rate does not change significantly over the entire angular range because the intended signal is nearly proportional to the interference at each AOA. However, at other locations, much more significant variation in ARAS can be found due to the "mismatch" between

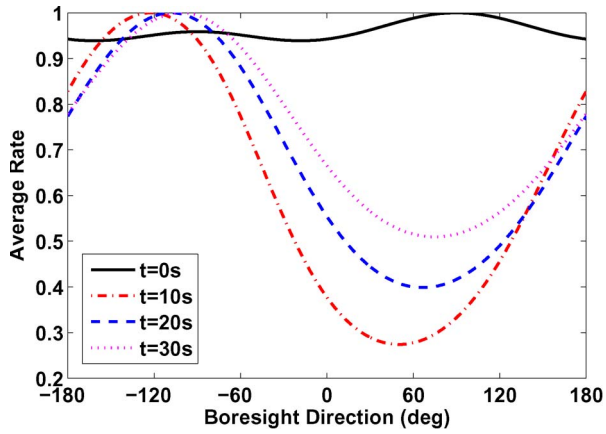

Fig. 11. ARAS (normalized with respect to the maximum values) obtained at the receiver $\mathbf{R}$ after it travels for 0, 10, 20, and 30 seconds.

the effective IAS and PAS. The more evident the mismatch, the more noticeable the ARAS variation. Finally, the boresight directions giving rise to the maximum average rate may change substantially as the receiver moves to different locations.

VII. Conclusion

We have presented the novel description method of IAS for characterizing network interference in the angular domain. We have also extended this concept to the directional modeling of average rate, and presented the notion of local area outage. Subsequently, we have proposed the GBSMs to support and enrich the description method. We have used several numerical examples to demonstrate the usefulness of the proposed analytical framework and highlight some interesting properties of the proposed interference performance measures. The results would provide useful insight on the design and evaluation of interference-prone network systems.

A future direction worthy of thinking is that interference also depends on specific multiple access, cooperation, and adaptive transmission schemes, which are the key aspects that differentiate the "smart" interferers from "dumb" scatterers. It would be interesting to incorporate these aspects into our model. Furthermore, it is useful to consider how to combine the Poisson point process methods and the GBSMs, which may allow the derivation of some new insights.

References

[1] M. Z. Win, P. C. Pinto, and L. A. Shepp, "A mathematical theory of network interference and its applications," *Proc. IEEE*, vol. 97, no. 2, pp. 205–230, Feb. 2009.

[2] K. Gulati, B. L. Evans, J. G. Andrews, and K. R. Tinsley, "Statistics of co-channel interference in a field of Poisson and Poisson-Poisson clustered interferers," *IEEE Trans. Signal Process.*, vol. 58, no. 12, pp. 6207–6222, Dec. 2010.

[3] H. S. Dhillon, R. K. Ganti, F. Baccelli, and J. G. Andrews, "Modeling and analysis of K-tier downlink heterogeneous cellular networks," *IEEE J. Sel. Areas Commun.*, vol. 30, no. 3, pp. 550–560, Apr. 2012.

[4] R. K. Ganti, J. G. Andrews, and M. Haenggi, "High-SIR transmission capacity of wireless networks with general fading and node distribution," *IEEE Trans. Inf. Theory*, vol. 57, no. 5, pp. 3100–3116, May 2011.

[5] R. K. Ganti, F. Baccelli, and J. G. Andrews, "Series expansion for interference in wireless networks," *IEEE Trans. Inf. Theory*, vol. 58, no. 4, pp. 2194–2205, Apr. 2012.

[6] S. Weber, J. G. Andrews, and N. Jindal, "An overview of the transmission capacity of wireless networks," *IEEE Trans. Commun.*, vol. 58, no. 12, pp. 3593–3604, Dec. 2010.
[7] R. K. Ganti and M. Haenggi, "Interference and outage in clustered wireless *Ad Hoc* networks," *IEEE Trans. Inf. Theory*, vol. 55, no. 9, pp. 4067–4086, Sep. 2009.
[8] A. Rabbachin, T. Q. S. Quek, H. Shin, and M. Z. Win, "Cognitive network interference," *IEEE J. Sel. Areas Commun.*, vol. 29, no. 2, pp. 480–493, Feb. 2011.
[9] J. Silvester and L. Kleinrock, "On the capacity of multihop slotted ALOHA networks with regular structure," *IEEE Trans. Commun.*, vol. 31, no. 8, pp. 974–982, Aug. 1983.
[10] R. Mathar and J. Mattfeldt, "On the distribution of cumulated interference power in Rayleigh fading channels," *Wireless Netw.*, vol. 1, no. 1, pp. 31–36, Feb. 1995.
[11] S. Catreux, P. F. Driessen, and L. J. Greenstein, "Simulation results for an interference-limited multiple-input multiple-output cellular system," *IEEE Commun. Lett.*, vol. 4, no. 11, pp. 334–336, Nov. 2000.
[12] A. Ganz, C. M. Krishna, D. Tang, and Z. J. Hass, "On optimal design of multitier wireless cellular systems," *IEEE Commun. Mag.*, vol. 35, no. 2, pp. 88–93, Feb. 1997.
[13] E. Ekici and C. Ersoy, "Multi-tier cellular network dimensioning," *ACM Wireless Netw.*, vol. 7, no. 4, pp. 401–411, Jul. 2001.
[14] M. Haenggi, J. G. Andrews, F. Baccelli, O. Dousse, and M. Franceschetti, "Stochastic geometry and random graphs for the analysis and design of wireless networks," *IEEE J. Sel. Areas Commun.*, vol. 27, no. 7, pp. 1029–1046, Sep. 2009.
[15] K. Gulati, R. K. Ganti, J. G. Andrews, B. L. Evans, and S. Srikanteswara, "Characterizing decentralized wireless networks with temporal correlation in the low outage regime," *IEEE Trans. Wireless Commun.*, vol. 11, no. 9, pp. 3112–3125, Sep. 2012.
[16] A. F. Molisch, *Wireless Communications*, 2nd ed. Chichester, U.K.: Wiley, 2010.
[17] K. I. Pedersen, P. E. Mogensen, and B. H. Fleury, "A stochastic model of the temporal and azimuthal dispersion seen at the base station in outdoor propagation environments," *IEEE Trans. Veh. Technol.*, vol. 49, no. 2, pp. 437–447, Mar. 2000.
[18] B. H. Fleury, "First- and second-order characterization of direction dispersion and space selectivity in the radio channel," *IEEE Trans. Inf. Theory*, vol. 46, no. 6, pp. 2027–2044, Sep. 2000.
[19] Y. Chen, S. Yang, and W. S. Wong, "Exact non-Gaussian interference model for fading channels," *IEEE Trans. Wireless Commun.*, vol. 12, no. 1, pp. 168–179, Jan. 2013.
[20] M. K. Simon and M.-S. Alouini, *Digital Communication over Fading Channels: A Unified Approach to Performance Analysis*. Hoboken, NJ, USA: Wiley, 2000.
[21] P. M. Shankar, *Fading and Shadowing in Wireless Systems*. New York, NY, USA: Springer-Verlag, 2012.
[22] S. Kandukuri and S. Boyd, "Optimal power control in interference-limited fading wireless channels with outage-probability specifications," *IEEE Trans. Wireless Commun.*, vol. 1, no. 1, pp. 46–55, Jan. 2002.
[23] J. F. Paris and D. Morales-Jimenez, "Outage probability analysis for Nakagami-q (Hoyt) fading channels under Rayleigh interference," *IEEE Trans. Wireless Commun.*, vol. 9, no. 4, pp. 1272–1276, Apr. 2010.
[24] J.-P. M. G. Linnartz, *Wireless Communication: The Interactive Multimedia CD-ROM*. New York, NY, USA: Springer-Verlag, 2001.
[25] M. Timmers, S. Pollin, A. Dejonghe, A. Bahai, L. Van der Perre, and F. Catthoor, "Accumulative interference modeling for cognitive radios with distributed channel access," in *Proc. IEEE CrownCom*, 2008, pp. 1–7.
[26] S. Kusaladharma and C. Tellambura, "Aggregate interference analysis for underlay cognitive radio networks," *IEEE Wireless Commun. Lett.*, vol. 1, no. 6, pp. 641–644, Dec. 2012.
[27] R. W. Heath and M. Kountouris, "Modeling heterogeneous network interference using Poisson point processes," *IEEE Trans. Signal Process.*, vol. 61, no. 16, pp. 4114–4126, Aug. 2013.
[28] M. D. Yacoub, J. E. V. Bautista, and L. G. de Rezende Guedes, "On higher order statistics of the Nakagami-m distribution," *IEEE Trans. Veh. Technol.*, vol. 48, no. 3, pp. 790–794, May 1999.
[29] G. D. Durgin and T. S. Rappaport, "Theory of multipath shape factors for small-scale fading wireless channels," *IEEE Trans. Antennas Propag.*, vol. 48, no. 5, pp. 682–693, May 2000.
[30] A. Papoulis and S. U. Pillai, *Probability, Random Variables and Stochastic Processes*. New York, NY, USA: MiGraw-Hill, 2002.
[31] J. Hamalainen, S. Savolainen, R. Wichman, K. Ruotsalainen, and J. Ylitalo, "On the solution of scatter density in geometry-based channel models," *IEEE Trans. Wireless Commun.*, vol. 6, no. 3, pp. 1054–1062, Mar. 2007.
[32] Y. Chen and V. K. Dubey, "Accuracy of geometric channel-modeling methods," *IEEE Trans. Veh. Technol.*, vol. 53, no. 1, pp. 82–93, Jan. 2004.
[33] R. J. Piechocki, J. P. McGeehan, and G. V. Tsoulos, "A new stochastic spatio-temporal propagation model (SSTPM) for mobile communications with antenna arrays," *IEEE Trans. Commun.*, vol. 49, no. 5, pp. 855–862, May 2001.
[34] R. B. Ertel and J. H. Reed, "Angle and time of arrival statistics for circular and elliptical scattering models," *IEEE J. Select. Areas Commun.*, vol. 17, no. 11, pp. 1829–1840, Nov. 1999.
[35] V. P. Mhatre, C. Rosenberg, D. Kofman, R. Mazumdar, and N. Shroff, "A minimum cost heterogeneous sensor network with a lifetime constraint," *IEEE Trans. Mobile Comput.*, vol. 4, no. 1, pp. 4–15, Jan./Feb. 2005.
[36] P. Petrus, J. H. Reed, and T. S. Rappaport, "Geometrical-based statistical macrocell channel model for mobile environments," *IEEE Trans. Commun.*, vol. 50, no. 3, pp. 495–502, Mar. 2002.

Yifan Chen (M'06) received the B.Eng. (Hons I) and Ph.D. degrees in electrical and electronic engineering from Nanyang Technological University (NTU), Singapore, in 2002 and 2006, respectively.

From 2005 to 2007, he was a Research Fellow with the Singapore-University of Washington Alliance (SUWA) in Bioengineering, supported by Singapore Agency for Science, Technology and Research (A∗STAR), NTU, and University of Washington at Seattle. From 2007 to 2012, he was a Lecturer and then a Senior Lecturer with University of Greenwich, U.K., and with Newcastle University, U.K. In 2013, he was a Visiting Professor with Singapore University of Technology and Design, Singapore. He is presently a Professor and Head of Department of Electrical and Electronic Engineering with South University of Science and Technology of China, Shenzhen. His current research interests include small- and multi-scale communications and sensing, transient wireless systems, microwave medical theranostics, wireless propagation and network channel modelling, and cognitive wireless systems.

Professor Chen received the Promising Research Fellowship in 2010 and the Early Career Research Excellence Award in 2009 from University of Greenwich. He was also selected by China's 8th Recruitment Program of Global Experts in 2012, received Guangdong Natural Science Funds for Distinguished Young Scholar in 2013, and was accredited Shenzhen Distinguished Overseas Talent in 2013. Professor Chen is the Coordinator of a European Commission FP7 project on intelligent medical ICT and an elected Working Group Co-leader of European COST Action TD1301 on microwave medical imaging. He also serves as the Technical Program Co-chair of 2014 IEEE International Conference on Consumer Electronics—China (ICCE-China).

Lorenzo Mucchi (M'98–SM'12) received the Dr. Eng. degree (Laurea) in telecommunications engineering from the University of Florence, Florence, Italy in 1998 and the Ph.D. degree in telecommunications and information society, in 2001.

Since 2001 he has been with the Department of Information Engineering of the University of Florence as a Research Scientist. In 2000 he spent a 12-months period of research at the Centre for Wireless Communications, University of Oulu, Finland. He is professor of Information Technologies at the University of Florence, Italy, since 2008. His main research areas include theoretical modelling, algorithm design and real measurements, mainly focused in the following fields: spread spectrum techniques (UWB, CDMA), localization, cooperative communications, cognitive radio, intrinsic wireless security, adaptive diversity techniques and multi-satellite communications. Currently, he has published 6 chapters in 6 different international books, 19 papers in international journals and several papers in international conference proceedings during his research activity.

Dr. Mucchi is senior member of the Institute of Electrical and Electronics Engineers (IEEE) and permanent member of the International Association of Science and Technology for Development (IASTED) Technical Committee on Telecommunications. Since 2004 he has been TPC for numerous international conferences. He has been Guest Editor and Editor-in-chief for the International Journal of Ultra Wide Band Communication Systems (IJUWBCS) and for Elsevier.

Rui Wang received the B.Eng. degree in computer science and engineering from the University of Science and Technology of China (USTC), Hefei, China, in 2004 and the Ph.D. degree in wireless communications from the Hong Kong University of Science and Technology (HKUST), Kowloon, Hong Kong, in 2008.

In 2009, he worked as a Post-Doctoral Research Associate in Hong Kong University of Science and Technology (HKUST), Kowloon. During 2009–2012, he worked as a Senior Research Engineer at Huawei-HKUST Innovation Laboratory, Huawei Technology, Co., Ltd. He is currently an Associate Professor in the South University of Science and Technology of China (SUSTC), Shenzhen, China.

Kaibin Huang (S'05–M'08–SM'13) received the B.Eng. (Hons I) and the M.Eng. degrees from the National University of Singapore, Singapore, in 1998 and 2000, respectively, and the Ph.D. degree from The University of Texas at Austin (UT Austin), Austin, TX USA, in 2008, all in electrical engineering.

Since Jan. 2014, he has been an Assistant Professor in the Department of Electrical and Electronic Engineering (EEE) at the University of Hong Kong. He is an Adjunct Professor in the School of EEE at Yonsei University in S. Korea. He used to be a Faculty Member in the Department of Applied Mathematics (AMA) at the Hong Kong Polytechnic University (PolyU) and the Department of EEE at Yonsei University. He had been a Postdoctoral Research Fellow in the Department of Electrical and Computer Engineering at the Hong Kong University of Science and Technology from June 2008 to February 2009 and an Associate Scientist at the Institute for Infocomm Research in Singapore from November 1999 to July 2004. His research interests focus on the analysis and design of wireless networks using stochastic geometry and multi-antenna techniques. He frequently serves on the technical program committees of major IEEE conferences in wireless communications. He chairs the Comm. Theory Symp. of IEEE GLOBECOM 2014 and the Adv. Topics in Wireless Comm. Symp. of IEEE/CIC ICCC 2014 and has been the technical co-chair for IEEE CTW 2013, the track chair for IEEE Asilomar 2011, and the track co-chair for IEEE VTC Spring 2013 and IEEE WCNC 2011. He is a guest editor for the IEEE JOURNAL ON SELECTED AREAS IN COMMUNICATIONS, an editor for the IEEE TRANSACTIONS ON WIRELESS COMMUNICATIONS, IEEE Wireless Communications Letters and also IEEE/KICS Journal of Communication and Networks. He is an elected member of the SPCOM Technical Committee of the IEEE Signal Processing Society.

Dr. Huang received the Outstanding Teaching Award from Yonsei, Motorola Partnerships in Research Grant, the University Continuing Fellowship from UT Austin, and Best Paper Awards from IEEE GLOBECOM 2006 and PolyU AMA in 2013.